JOURNAL OF MATERIALS SCIENCE 17 (1982) 580–588

Production of Fe–P–C amorphous wires by in-rotating-water spinning method and mechanical properties of the wires

A. INOUE, M. HAGIWARA*, T. MASUMOTO
The Research Institute for Iron, Steel and Other Metals, Tohoku University, Sendai 980, Japan.

Continuous amorphous wires with high strength and good ductility have been produced in the Fe–P–C alloy system by the in-rotating-water spinning technique; however, no amorphous wires are formed, using the same technique, in the Fe–P–B, Fe–P–Si and Fe–B–C systems. The Fe–P–C amorphous wires have a circular cross-section, smooth peripheral surface, and diameters in the range of about 80 to 230 μm. Their tensile strength, σ_f, and Vickers hardness, H_v, increase with increasing phosphorus and/or carbon content and reach 3000 MPa and 895 DPN for $Fe_{75}P_{10}C_{15}$. Fracture elongation, ϵ_f, including elastic elongation is about 2.8%. Cold-drawing to an appropriate reduction in area causes an increase in σ_f and ϵ_f of about 3.7 and 79%, respectively. This increase is interpreted to result from an interaction between crossing deformation bands introduced by cold-drawing and the increase in the uniformity of shape for the drawn wires. Further, the undrawn and drawn amorphous wires are so ductile that no cracks are observed even after a sharp bending test. Thus, the Fe–P–C amorphous wires are attractive for fine-gauge high-strength materials both because of the uniform shape of the wires and because of their superior mechanical qualities.

1. Introduction

It is well known (see, for example, [1]) that iron-based amorphous alloys produced by melt-quenching possess high strength as well as ductility. However, almost all the iron-based amorphous alloys which are produced by conventional melt-quenching techniques are ribbon-shaped; this shape limits applications as a high-strength material. Therefore, in order to make the best use of the good mechanical properties of these alloys, it was necessary to develop a method for the production of an amorphous wire with a circular cross-section. Recently, the present authors have succeeded in producing continuous amorphous wires with almost completely circular cross-sections for Fe–Si–B [2] and Co–Si–B [3] alloys as well as Pd–Cu–Si [4] alloys by the modified melt-spinning technique [5], in which a melt stream is ejected into a rotating water layer, and have shown that the Fe–Si–B and Co–Si–B amorphous wires have high-strength combined with good ductility which exceeds the values for heavily cold-drawn steel wires. In the subsequent investigations, it has been found [6] that the continuous amorphous wires are also formed in the Fe–P–C system by using the newly-developed quenching technique. This paper deals with the formation tendency of an amorphous wire in the Fe–P–C, Fe–P–B, Fe–B–C and Fe–P–Si systems and the mechanical properties and thermal stability of the amorphous wires.

2. Experimental details

The specimens used in the present work are $Fe_xP_yC_z$, $Fe_xP_yB_z$, $Fe_xB_yC_z$ and $Fe_xP_ySi_z$ ternary alloys. Mixtures of electrolytic iron and

*Present address: Unitika Research Centre, Unitika Ltd, Uji 611, Japan.

0022–2461/82/020580–09$2.90/0

pure metalloids (boron, carbon, phosphorus and/or silicon) were melted under an argon atmosphere in an induction furnace. The melt was sucked up into a quartz tube of inside diameter about 3 mm and solidified in the tube. The compositions were expressed by the weighed values in atomic per cent since the difference between weighed and chemically-analysed compositions was less than 0.10 wt% for carbon, 0.2 wt% for phosphorus and 0.5 wt% for silicon.

Continuous amorphous wires with various diameters between 0.1 and 0.2 mm were prepared from these master alloys by an in-rotating-water spinning apparatus in which the melt was ejected through the orifice into the rotating water layer. The details of the apparatus are described in [4]. Typically, the amount of alloy melted in one run was about 1 g, the rotation speed of the drum (50 cm in diameter) was controlled to be 200 to 400 rpm and the depth of the cooling water was about 2.5 cm.

Identification of the as-quenched phases was made using the Debye–Scherrer X-ray method, using manganese-filtered FeKα radiation, and transmission electron microscopy. The wires were determined to be amorphous when the X-ray intensity as a function of diffraction angle showed a typical liquid-like structure. The hardness and tensile strength of the wires were measured by a Vickers microhardness tester with a 100 g load and an Instron-type tensile testing machine at a strain rate of $4.7 \times 10^{-4}\,\mathrm{sec}^{-1}$, respectively. Tensile specimens were cut out from undrawn and drawn long wires into the short pieces having the gauge dimension of 20 mm length. A specially designed set of grips for the small filament was used to insure proper specimen alignment within the machine. Subsequent to tensile testing, the cross-sectional area at the fracture site of each specimen was measured using optical microscopy. This procedure was followed to minimize error in estimation of the tensile strength. Young's modulus was determined from the slope within the elastic limit on the stress–elongation curve. The crystallization temperature was measured at a heating rate of about $0.08\,\mathrm{K\,sec}^{-1}$ by a differential thermal analyser (DTA), and the activation energy for crystallization was examined using a differential scanning calorimeter (DSC) at various heating rates in the range 0.0833 to $1.33\,\mathrm{K\,sec}^{-1}$. Ductility was evaluated by measuring the radius of curvature at fracture in a simple bend test. The peripheral

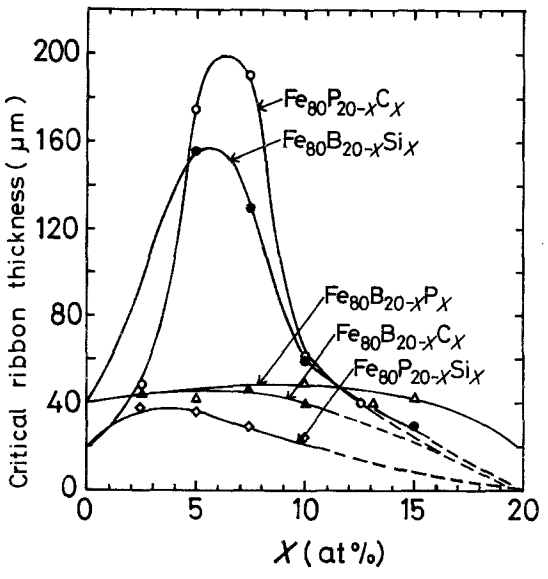

Figure 1 Compositional dependence of the critical ribbon thickness for the formation of an amorphous single-phase in $Fe_{80}(P{-}C)_{20}$, $Fe_{80}(P{-}B)_{20}$, $Fe_{80}(P{-}Si)_{20}$ and $Fe_{80}(B{-}C)_{20}$ alloys.

structure before and after drawing and the fracture surface were observed using a scanning electron microscope.

3. Results and discussion

3.1. The glass-forming tendency of iron-based amorphous alloys

With a view to obtaining information on the degree of glass-forming tendency which is necessary for the production of an amorphous wire, we measured the critical sample thickness for the formation of an amorphous phase in Fe–P–C, Fe–P–B, Fe–P–Si and Fe–B–C alloys using a melt-spinning-type quenching apparatus which enables the copper roller (20 cm in diameter) revolving at high speeds (3000 to 5000 rpm) to stop in a very short time (1 to 2 sec). The details of this apparatus and the method for the determination of the critical thickness are described in [7]. Fig. 1 shows the results for $Fe_{80}(P{-}C)_{20}$, $Fe_{80}(P{-}B)_{20}$, $Fe_{80}(P{-}Si)_{20}$ and $Fe_{80}(B{-}C)_{20}$ ternary alloys. Also, the data for $Fe_{80}(Si{-}B)_{20}$ alloys [8] are represented in the Fig. 1 for comparison. The critical thickness was taken as that thickness where a crystalline particle was just observed by optical microscope at magnification of times 100. The justification for such an identification by optical microscopy was also confirmed by X-ray analysis. As shown in Fig. 1, the highest

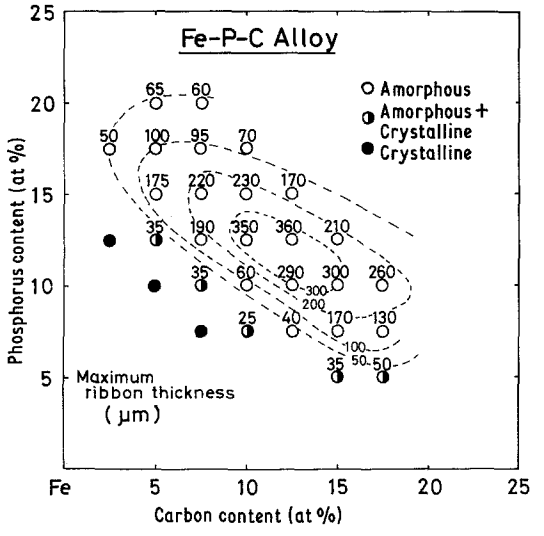

Figure 2 Compositional dependence of the critical ribbon thickness for the formation of an amorphous single-phase in Fe–P–C ternary alloys.

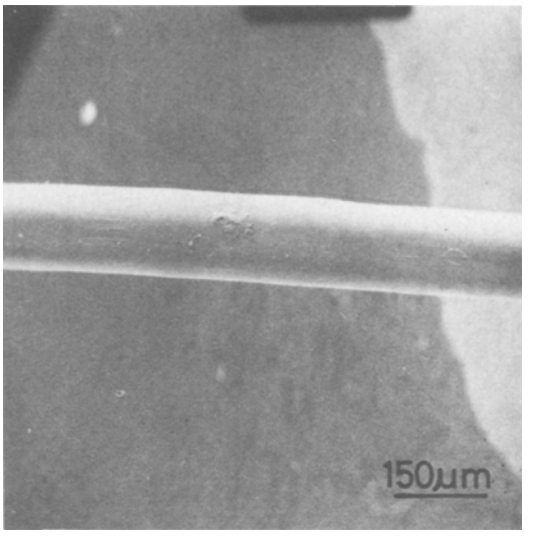

Figure 3 Scanning electron micrograph showing the peripheral surface of as-quenched $Fe_{77.5}P_{12.5}C_{10}$ amorphous wire.

critical ribbon thickness is about 200 μm for $Fe_{80}(P–C)_{20}$, 50 μm for $Fe_{80}(P–B)_{20}$, 35 μm for $Fe_{80}(P–Si)_{20}$ and 45 μm for $Fe_{80}(B–C)_{20}$, indicating that the glass-forming tendency is largest for Fe–P–C followed by Fe–P–B, Fe–B–C and then Fe–P–Si. Thus, the glass-forming tendency of Fe–P–C alloys is almost equal to that of Fe–Si–B alloys and is much larger than those of the other alloy systems.

With a view to finding the alloy composition possessing the largest glass-forming ability, we measured the critical sample thickness for the formation of an amorphous phase for Fe–P–C alloys with various metalloid compositions and the result is shown in Fig. 2. The largest value of the critical thickness is about 360 μm around the $Fe_{75}P_{12.5}C_{12.5}$ composition and the values near the boundary between amorphous and crystalline phases are in the range of about 30 to 40 μm. The critical thicknesses of Fe–P–C alloys having the metalloid contents above about 26 at% are not represented in Fig. 2, in spite of the expectation that the alloys exhibiting a large critical thickness might be formed for the Fe–P–C alloys containing higher metalloid contents. This omission is due to the fact that the melting of the alloys becomes more difficult with increasing carbon and phosphorus contents because of the high melting point of alloys and the ease of evaporation of phosphorus and carbon. Anyhow, it is to be noticed that the Fe–P–C alloys exhibit an amorphous single phase even in the ribbon as thick as about 360 μm which exceeds the largest critical thickness (250 μm) [8] for the Fe–Si–B system. This result suggests the possibility that the continuous amorphous wire with diameters of between 100 and 200 μm is also formed in the Fe–P–C system.

3.2. Production of amorphous wires

A continuous amorphous wire with almost completely circular cross-section and smooth surface was produced in the Fe–P–C system by the modified melt-spinning apparatus using rotating water as the cooling medium. Fig. 3 shows a typical scanning electron micrograph of the peripheral surface of $Fe_{77.5}P_{12.5}C_{10}$ amorphous wires. Variation of the wire diameter is about 10% for the wire approximately 150 μm in diameter and tends to decrease with decreasing wire diameter. Thus, the iron-based amorphous wires produced by this technique possess a good uniformity of shape, indicating the high stability of the molten jet in rotating water. Additionally, the above results indicate that the melt ejected through the nozzle was supercooled below the glass transition temperature, T_g, of the alloy without any disruption of the stable jet stream, even in a liquid medium such as rotating water. The other quenching parameters, for the production of Fe–P–C amorphous wires with good shape and uniformity, were adjusted as follows: (1) The distance between the surface of the water and the end of the quartz tube was less than about 3 mm and the angle of

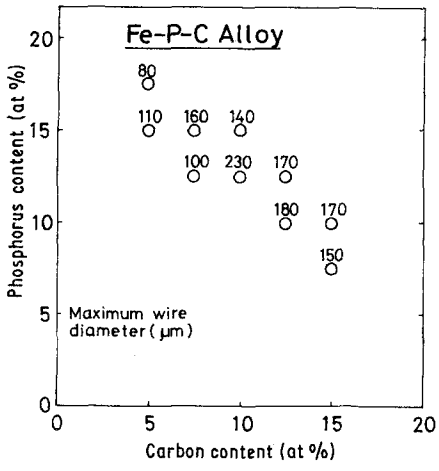

Figure 4 Maximum diameter for the formation of an amorphous wire in Fe–P–C ternary alloys.

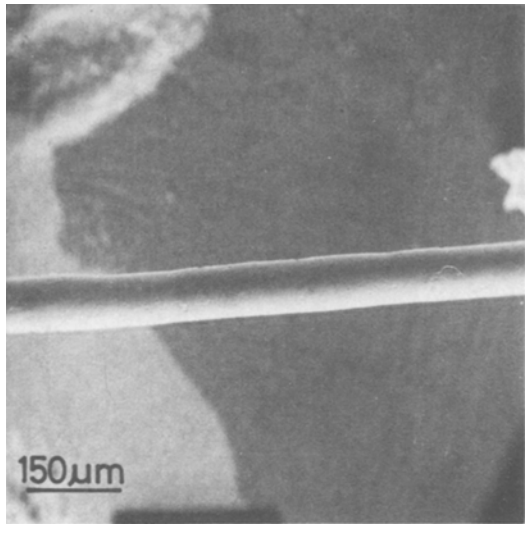

Figure 5 Scanning electron micrograph showing the peripheral surface of as-quenched $Fe_{80}P_{10}Si_{10}$ wire.

the nozzle against the surface of water was about 60°; (2) the inner diameter of the ruby nozzle was varied between 0.1 and 0.3 mm; (3) the temperature of the cooling water was approximately 278 K; and (4) the melt was ejected by an argon pressure of about 0.35 MPa from a temperature about 75 K above the liquidus temperature and its ejected speed was estimated to be about 500 m min^{-1}. Additionally, it is required that the water velocity in the drum exceeds the jet velocity by about 15 to 25%.

Fig. 4 shows the maximum diameter for the formation of an amorphous wire of some Fe–P–C alloys. The largest value of about 230 μm is seen around $Fe_{77.5}P_{12.5}C_{10}$ and it tends to decrease with increasing or decreasing phosphorus and carbon contents. Such a compositional dependence agrees well with that of the critical thickness for the formation of the amorphous ribbon, shown in Fig. 2. This result suggests that the larger the critical thickness, the higher is the formation tendency of an amorphous wire, similar to the tendency of formation of Fe–Si–B [2] and Co–Si–B [3] amorphous wires.

A continuous wire with circular cross-section and smooth surface was also formed in the Fe–P–Si system under the above-described condition, as shown in Fig. 5. However, the wire exhibited a crystalline phase owing to the low glass-forming tendency of the alloys and no amorphous wire could be formed at any alloy compositions in the Fe–P–Si system. On the other hand, rapidly quenched Fe–P–B alloys exhibited two kinds of distinctly different form, as exemplified in Fig. 6. One form is a discontinuous wire with axisymmetrical nodes for the $Fe_{80}P_{15}B_5$ alloy, and the other form is small balls with diameter about 150 μm for $Fe_{80}P_{13}B_7$ alloy. The two kinds of quenched samples consisted of a duplex structure of amorphous and crystalline phases. The above result indicates that the tendency to form a wire becomes enhanced with increasing phosphorus and silicon contents. As expected, all the quenched Fe–B–C alloys exhibited the form of small balls, as shown in Fig. 7 and hence it is concluded that the wire-forming tendency of Fe–B–C alloys is much lower compared with the other alloys containing phosphorus and/or silicon elements. The remarkable enhancement in the wire formation tendency by the addition of phosphorus and/or silicon is considered to be closely related to the fact [9] that the dissolution of phosphorus and/or silicon causes a remarkable increase in the viscosities of the molten alloys. It is empirically known, see for example [10], that the formation tendency of an amorphous wire is enhanced with increased viscosity or decreased surface tension of the molten alloys.

3.3. Mechanical properties of Fe–P–C amorphous wires

3.3.1. Compositional dependence of mechanical properties

The compositional dependences of tensile strength, σ_f, fracture elongation, ϵ_f, including elastic

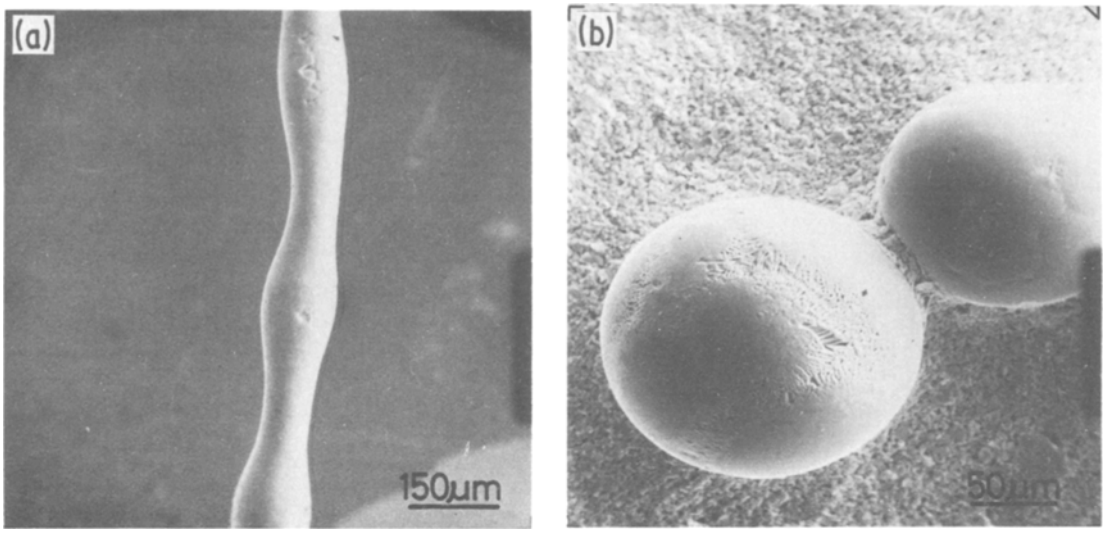

Figure 6 Scanning electron micrographs showing the form of as-quenched (a) $Fe_{80}P_{15}B_5$ and (b) $Fe_{80}P_{13}B_7$ alloys.

elongation, Vickers hardness, H_v, and crystallization temperature, T_x for undrawn and drawn Fe–P–C amorphous wires having diameter of about 100 μm are shown in Figs 8 to 11. Here, the strength values are the average over five specimens and the T_x is the temperature determined as being the starting point of the first exothermic peak on the DTA curve. The σ_f, H_v and T_x values for the undrawn wires increase with increasing phosphorus and/or carbon contents and reach about 3000 MPa, 895 DPN and 706 K, respectively, for $Fe_{75}P_{10}C_{15}$. The effect of metalloid elements on the increases in σ_f and H_v is much larger for carbon than for phosphorus, similar to the tendency [11] for Fe–P–C amorphous ribbons. Also, the ϵ_f value of these undrawn amorphous wires is about 2.8% and a definite compositional dependence of the ϵ_f is not seen. Young's modulus, E, is of the order 9.8×10^4 MPa. As described above, the σ_f value was measured for the amorphous wires having a diameter of about 100 μm. It has been demonstrated for Fe–Si–B amorphous wires [2] that there is hardly any change in strength with varying wire diameter in the range from 70 to 230 μm. Therefore, it may be concluded that the high strength of the Fe–P–C amorphous wires is not due to their small diameter, but is due to the inherent nature of the amorphous structure.

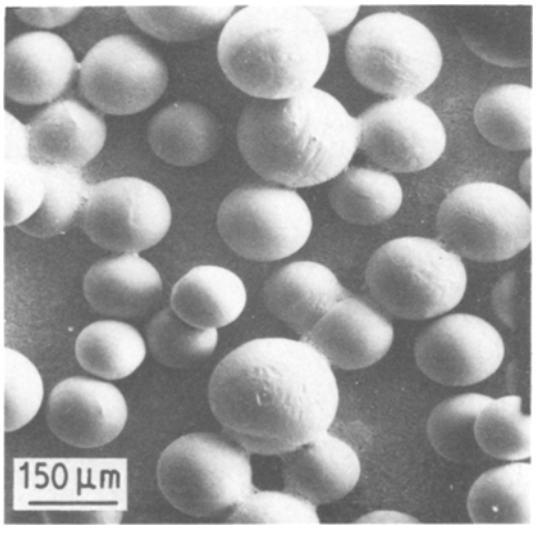

Figure 7 Scanning electron micrograph showing the form of as-quenched $Fe_{80}B_{10}C_{10}$ alloy.

3.3.2. The effect of cold drawing on mechanical properties

Next, the limiting feasible area reduction of some Fe–P–C amorphous wires by cold-drawing was examined, which is a very important factor for practical applications. For example, the $Fe_{77.5}P_{12.5}C_{10}$ amorphous wire could be cold-drawn from about 150 μm to 60 μm in diameter after multiple passes through several diamond dies without annealing treatments. In the cold-drawing, soapy water was used as a lubricant. Furthermore, the Fe–P–C amorphous wires possess a good bend ductility, even after cold-drawing as severe as about 90% reduction in cross-sectional area. As an example, scanning electron micrographs showing the deformation structure of the cold-drawn

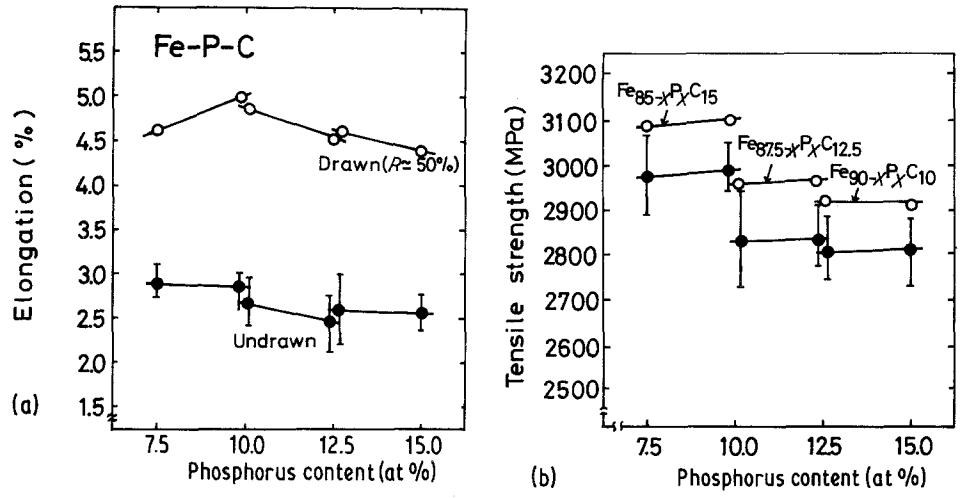

Figure 8 Variation in (a) the tensile strength σ_f, and (b) the fracture elongation, ϵ_f, of undrawn and drawn Fe–P–C amorphous wires with P-content.

$Fe_{77.5}P_{12.5}C_{10}$ amorphous wire, bent through 180° by pressing against the edge of a razor blade, is shown in Fig. 12. Two families of deformation steps appear near the bent edge: one makes an angle of almost 45 to 50° to the longitudinal direction of the wire, while the other lies nearly perpendicular to it. A large number of the slip markings intersect each other and some are terminated by others, but no cracks are observed even after such a severe deformation.

Changes in E, σ_f and ϵ_f before and after drawing for the $Fe_{77.5}P_{12.5}C_{10}$ amorphous wire possessing the original diameter of about 150 μm are shown in Fig. 13 as a function of the total reduction in cross-sectional area. E increases from 9.8×10^4 to 11.1×10^4 MPa with the amount of reduction in area. σ_f is about 2800 MPa for the undrawn state, increases gradually with increasing reduction in area, reaches the maximum value (3000 MPa) for the drawn state at 60 to 70% reduction and tends to decrease with further reduction in area. Similarly, the ϵ_f value increases from about 2.8% to 4.7% by light drawing to 25 to 35% reduction, remains almost unchanged up to about 60% reduction and decreases rapidly with further increasing reduction in area. Additionally, the changes in the σ_f and ϵ_f values of Fe–P–C amorphous wires having different metalloid compositions by cold-drawing to about 50% reduction in area are presented in Figs 6 and 7.

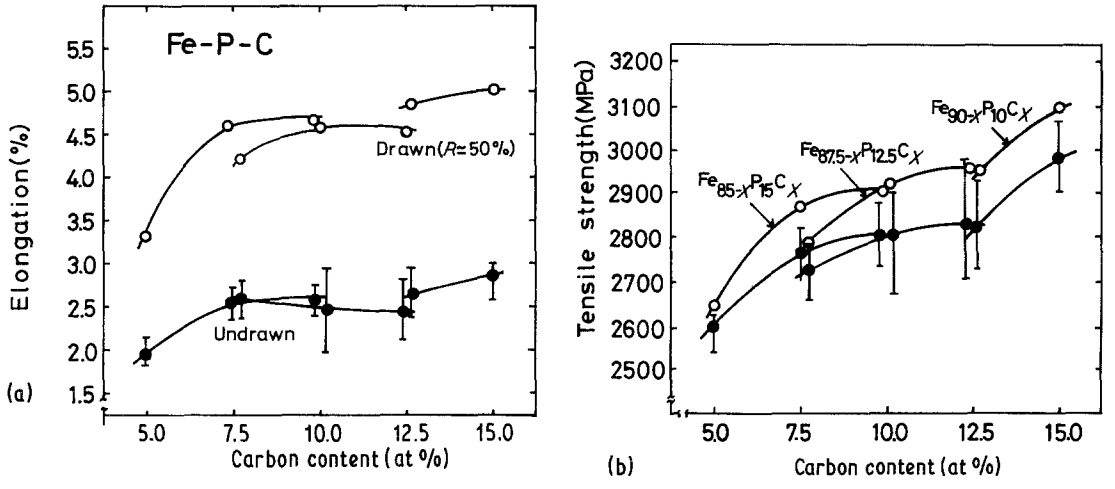

Figure 9 Changes in (a) the tensile strength, σ_f, and (b) the fracture elongation, ϵ_f, of undrawn and drawn Fe–P–C amorphous wires with C-content.

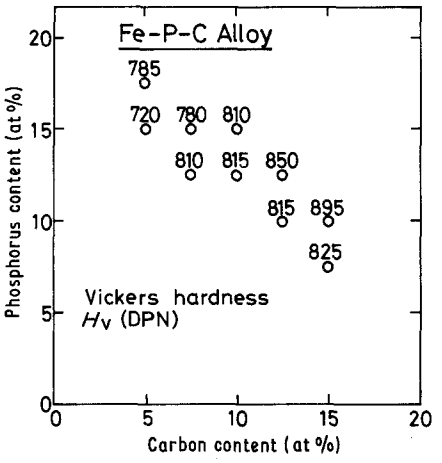

Figure 10 Compositional dependence of the Vickers hardness, H_v, of Fe–P–C amorphous alloys.

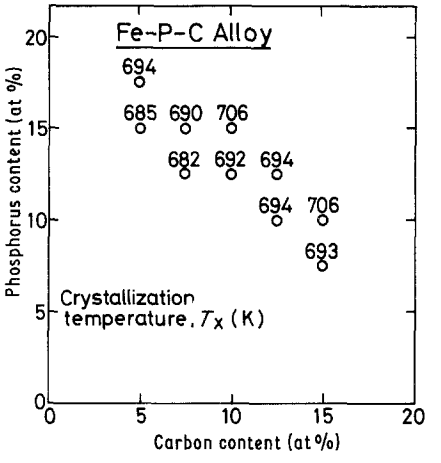

Figure 11 Compositional dependence of the crystallization temperature, T_x, of Fe–P–C amorphous alloys.

Thus, the σ_f and ϵ_f values for the Fe–P–C amorphous wires increase definitely by cold-drawing to an appropriate reduction in area. The high tensile strength (about 3100 MPa) of Fe–P–C amorphous wires is almost equal to the highest value of the conventional high-strength steel wires, even though the strength is considerably lower than that of Fe–Si–B and Co–Si–B amorphous wires. Such changes in σ_f and ϵ_f before and after drawing are similar to those observed for $Pd_{77.5}Cu_6Si_{16.5}$, $Fe_{75}Si_{10}B_{15}$ and $Co_{72.5}Si_{12.5}B_{15}$ amorphous wires produced by the same technique. The increases in the σ_f and ϵ_f produced by moderate cold drawing are considered not to be due to the structural change in the amorphous phase but to result from the two following changes:

(a) the inhibition of further deformation by an interaction among a number of deformation bands; and

(b) an increase of uniformity of shape by drawing. On the other hand, the eventual decreases in σ_f and ϵ_f produced by heavy drawing are considered to be due to nucleation and growth of voids or cracks at the points of intersection of crossing deformation bands.

The ratio $E/\sigma_f \simeq 35$ may be compared with that for iron whiskers, $E/\sigma_f \simeq 15$ [12]. Also, the ratio H_v/σ_f (DPN/kg mm^{-2}) is almost equal to 3.0, as expected for amorphous alloys in which the indentation is accompanied by a large compressive plastic flow with little strain-hardening [13].

3.3.3. Fracture morphology

Tensile fracture of the undrawn and drawn amorphous wires occurs on the shear plane at 45 to 50° to the tensile axis. The fracture surface consists of a smooth and featureless zone, produced by shear slip, and a vein-pattern of local necking protrusions, produced during rupture. Such a fracture pattern remains unchanged before and after drawing, as shown in Fig. 14. These results indicate that the fracture of Fe–P–C amorphous wires proceeded by highly localized shear deformation. These characteristics of fracture appearance are similar to those of Pd–Cu–Si [4], Fe–Si–B [2] and Co–Si–B [3] amorphous wires.

4. Summary

Continuous amorphous wires exhibiting high strength and good bend ductility were produced for the alloys possessing high glass-forming ability in the Fe–P–C system; however, no amorphous wires were formed in the Fe–P–B, Fe–P–Si and Fe–B–C alloy systems because of their poor glass-forming ability. The production of an amorphous wire was carried out using the modified melt-spinning apparatus in which the melt was ejected through the orifice of ruby nozzle into rotating water. The maximum diameter of the Fe–P–C amorphous wires was about 230 μm. The wires have a circular cross-section and a very smooth peripheral surface. Tensile strength, σ_f, and Vickers hardness, H_v, for the undrawn wires increase from 2600 to 3000 MPa and from 720 to 895 DPN, respectively, with increasing phosphorus and/or carbon content. The fracture elongation, ϵ_f, including elastic elongation, is about 2.5%. By cold-drawing to an appropriate reduction in area,

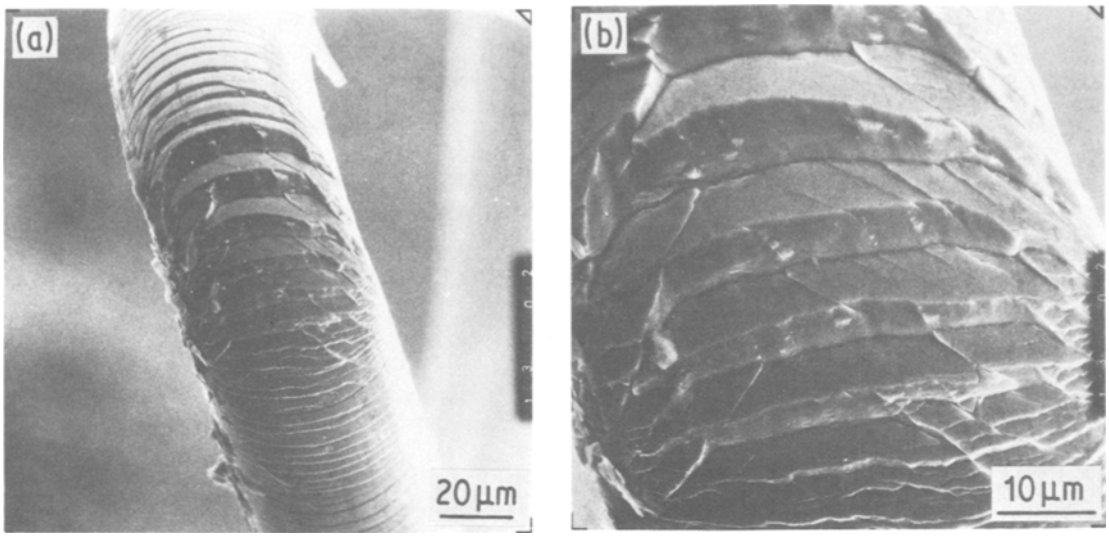

Figure 12 Scanning electron micrographs showing the deformation marking at the tip of an $Fe_{77.5}P_{12.5}C_{10}$ amorphous wire bent through 180° after cold-drawing to 40% reduction.

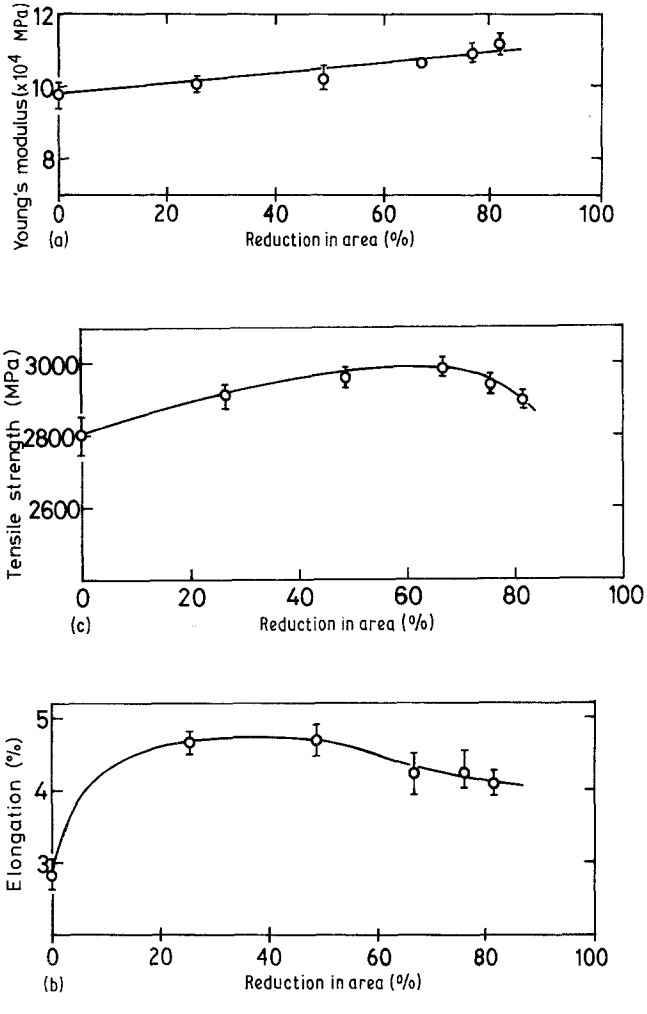

Figure 13 Changes in the Young's modulus, E, tensile strength, σ_f, and fracture elongation, ϵ_f, of $Fe_{77.5}P_{12.5}C_{10}$ amorphous wire with varying cold-drawn reduction in area.

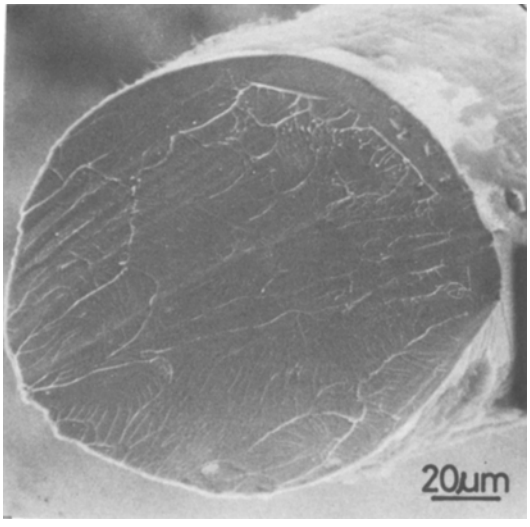

Figure 14 Scanning electron micrograph showing the tensile fracture appearance of $Fe_{77.5}P_{12.5}C_{10}$ amorphous wire cold-drawn to 40% reduction.

the σ_f and ϵ_f values of the Fe–P–C amorphous wires increase by about 7 and 68%, respectively, e.g. σ_f increases from 2800 to 3000 MPa and ϵ_f increases from 2.8 to 4.7% for $Fe_{77.5}P_{12.5}C_{10}$. Such increases are considered to result from preventing further deformation by an interaction among numerous deformation bands introduced by cold-drawing and an increase in the uniformity of shape by drawing. Further, the undrawn and drawn amorphous wires are so ductile that no cracks are observed, even after closely contacted bending test. In conclusion, it may be stated that the Fe–P–C amorphous wires are very attractive for use as high-strength materials because of their circular cross-section, their high tendency to form an amorphous wire, their high strength combined with good bend ductility and their inexpensiveness. Because of these advantages, the Fe–P–C amorphous wires are expected to be used hereafter as practical fine-gauge high-strength wires.

Acknowledgements

The authors would like to thank Mr. K. Yasuhara and Mr H. Tomioka of Unitika Ltd for carrying out some of the experimental work.

References

1. T. MASUMOTO, *Mater. Sci. Eng.* **19** (1975) 1.
2. M. HAGIWARA, A. INOUE and T. MASUMOTO, unpublished work.
3. *Idem,* unpublished work.
4. T. MASUMOTO, I. OHNAKA, A. INOUE and M. HAGIWARA, *Scripta Met.* **15** (1981) 293.
5. I. OHNAKA, Japanese Patent, Laid-Open Application, number 64948, 1980.
6. T. MASUMOTO, A. INOUE, M. HAGIWARA, I. OHNAKA and T. FUKUSAKO, Proceedings of the 4th International Conference on Rapidly-Quenched Metals, Sendai, August 1981.
7. M. HAGIWARA, A. INOUE and T. MASUMOTO, *Met. Trans. A* **12** (1981) 1027.
8. *Idem, Sci. Rep. Res. Inst. Tohoku Univ.* **A29** (1981) 351.
9. Y. NISHI, H. WATANABE, K. SUZUKI and T. MASUMOTO, *J. de Phys. Colloque-8* **41** (1980) 359.
10. S. KAVESH, "Metallic Glasses", edited by H. J. Leamy and J. J. Gilman, (American Society for Metals, Metals Park, Ohio, 1976) p. 36.
11. M. NAKA and T. MASUMOTO, *Sci. Rep. Res. Inst. Tohoku Univ.,* A-27 (1979) 118.
12. S. S. BRENNER, *J. Appl. Phys.* **27** (1956) 1484.
13. R. HILL, "The Mathematical Theory of Plasticity" (Oxford University Press, London, 1967) p. 213.

Received 24 June
and accepted 20 July 1981